Large eddy simulation of ocean mesoscale eddies

By P. Perezhogin†, A. Balakrishna AND R. Agrawal

Mesoscale eddies produce lateral (2D) fluxes that need to be parameterized in eddy-permitting $(1/4°)$ global ocean models due to insufficient spatial resolution. Here, we systematically apply methods from the 3D LES community to parameterize vorticity fluxes produced by mesoscale eddies leveraging an explicit filtering approach together with a dynamic procedure. The developed subfilter closure is implemented into the GFDL MOM6 ocean model and is evaluated in an idealized configuration, Double Gyre, both *a-priori* and *a-posteriori*. For sufficiently resolved grids, the LES simulations converge to the filtered high-resolution data. However, limitations in the proposed closure are observed when the filter scale approaches the energy-containing scales: the *a-priori* performance drops and *a-posteriori* experiments fail to converge to the filtered high-resolution data. Nevertheless, the proposed closure is accurate in predicting the mean flow in *a-posteriori* simulations at all resolutions considered $(1/2° − 1/8°)$. Finally, we propose parameterizing the thickness fluxes using a Bardina model which further improves simulations at the coarsest resolutions $(1/2° − 1/3°)$.

1. Introduction

Traditional parameterizations of mesoscale eddies attempt to close the energy budget by parameterizing dissipation and backscatter of kinetic energy (Jansen & Held 2014) and removal of the potential energy (Gent & McWilliams 1990). However, these parameterizations are commonly tuned to maximize *a-posteriori* performance, and consequently, their *a-priori* accuracy and connection to high-resolution data are unknown. In recent years there has been a substantial effort to develop mesoscale parameterizations with high *a-priori* accuracy by applying the large eddy simulation (LES) paradigm (Fox-Kemper & Menemenlis 2008; Khani & Dawson 2023) or machine learning methods (Zanna & Bolton 2020). However, as compared to studies of 3D turbulence, the assessment of these methods has been limited thus far. For instance, the dynamic model of Germano *et al.* (1991) has been evaluated in ocean models only once (Bachman *et al.* 2017).

Vorticity fluxes (or momentum fluxes) in quasi-2D fluids are responsible for the forward cascade of enstrophy and inverse cascade of energy. Thus, careful consideration of both dissipation and backscatter is required to produce accurate and numerically stable subfilter closures. Perezhogin & Glazunov (2023) showed that the 3D LES closure of Horiuti (1997) can be adapted for the prediction of vorticity fluxes in 2D decaying turbulence. In particular, the Reynolds stress, which is a part of the Germano (1986) decomposition, is responsible for additional kinetic energy backscatter. This finding was further confirmed and exploited by Perezhogin *et al.* (2023) in an idealized GFDL MOM6 ocean model (Adcroft *et al.* 2019). However, subfilter closures in that work were subject to substantial *a-posteriori* tuning, and thus assessing their *a-priori* accuracy is challenging.

† Courant Institute of Mathematical Sciences, New York University

In this light, we propose a methodology for parameterization of mesoscale eddies in the MOM6 ocean model that addresses a problem of *a-posteriori* tuning without degrading *a-priori* accuracy. We utilize two approaches adopted by the three-dimensional LES community, namely the explicit filtering approach (Winckelmans *et al.* 2001; Bose *et al.* 2010) and the dynamic procedure of Germano *et al.* (1991). Following the explicit filtering approach, we assume that the LES filter width $\overline{\Delta}$ is larger than the LES grid spacing Δx. This improves our predictions of the subfilter flux by allowing a partial inversion of the LES filter (Carati *et al.* 2001). Additionally, we suppress the numerical discretization errors by increasing the filter-to-grid width ratio (FGR $= \overline{\Delta}/\Delta x$). Finally, the "dynamic procedure" allows us to accurately estimate the free parameters of the parameterization from the resolved flow only. Overall, our approach permits a parameterization with good *a-priori* accuracy and contains a single tunable parameter FGR, which is adjusted to maximize the *a-posteriori* performance.

The rest of this report is organized as follows. Section 2 describes the MOM6 ocean model, the subfilter closure of vorticity fluxes (Perezhogin & Glazunov 2023) and a newly proposed closure of thickness fluxes. In Section 3 we show *a-priori* and *a-posteriori* results and compare it to high-resolution filtered data. Finally, concluding remarks are made in Section 4.

2. Methods

Here we attempt to improve the dynamical core of the MOM6 ocean model, which solves the stacked shallow water equations, with improved LES subfilter closures.

2.1. *Double Gyre configuration*

The stacked (i.e., multilayer) shallow water equations in the vector-invariant form are given as,

$$\partial_t u^k - (\omega^k + f)v^k + \partial_x(K^k + M^k) = \mathcal{F}_x^k, \tag{2.1}$$

$$\partial_t v^k + (\omega^k + f)u^k + \partial_y(K^k + M^k) = \mathcal{F}_y^k, \tag{2.2}$$

$$\partial_t h^k + \partial_x(u^k h^k) + \partial_y(v^k h^k) = 0, \tag{2.3}$$

where k is the index of the fluid layer, u^k and v^k are zonal and meridional velocities and h^k is the thickness of the fluid layer. Further, $\omega^k = \partial_x v^k - \partial_y u^k$ is the relative vorticity, $K^k = 1/2((u^k)^2 + (v^k)^2)$ is the kinetic energy per unit mass and M^k is the Montgomery potential (pressure anomaly). Also, f is the Coriolis parameter and $\mathcal{F}^k$ is an additional forcing and dissipation. Note that there is no horizontal molecular viscosity in these equations and thus the small-scale dissipation is provided by the subgrid parameterization only.

We consider an idealized configuration Double Gyre of GFDL MOM6 ocean model described in Perezhogin *et al.* (2023) and shown in Figure 1. Two fluid layers are governed by the stacked shallow water equations (Eqs. (2.1)-(2.3)), with $\mathcal{F}^k$ given by a wind stress applied at the surface and a drag force applied at the ocean floor. The model domain is on a sphere with a spatial extent of $(0°-22°E) \times (30°-50°N)$ which is approximately 2000 km × 2000 km. We run experiments for 20 years of model time and use the last 10 years for computation of statistics to isolate from the transient development.

The high-resolution simulation at resolution $1/64°$ resolves the mesoscale eddies with 10 grid points as its grid spacing (1.5 km) is 10 times smaller than the first baroclinic
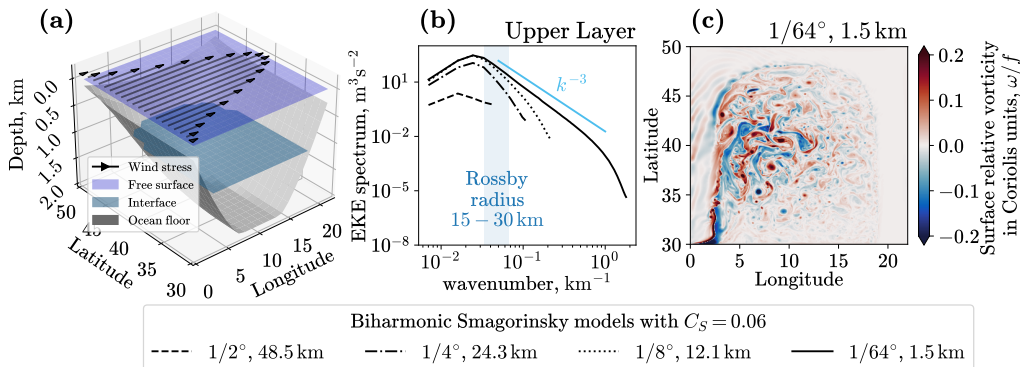
FIGURE 1. Idealized configuration Double Gyre of GFDL MOM6 ocean model: (a) schematic, (b) spatial spectrum of eddy kinetic energy (EKE) in a box $(5° − 15°E) \times (35° − 45°N)$ in upper fluid layer, (c) snapshot of vorticity in high-resolution model.

Rossby radius $(15 − 30$ km), the scale at which mesoscale eddies are generated (see blue shading in Figure 1(b)). In contrast, ocean models with the coarsest resolutions considered $(1/2°$ and $1/4°)$ have an insufficient number of grid points per Rossby radius, leading to insufficient eddy energy across all spatial scales (Figure 1(b)). In these baseline experiments, we parameterize the subgrid momentum fluxes with the biharmonic Smagorinsky model having a coefficient of $C_S = 0.06$, which is a default value in the global ocean model (Adcroft *et al.* 2019). Smaller values of C_S are possible but will lead to the appearance of numerical noise in the vorticity field. The mentioned lack of eddy energy is caused by the too-strong dissipation provided by the biharmonic Smagorinsky parameterization. The remainder of this report focuses on replacing this parameterization with alternative subgrid models to enhance the coarse-resolution ocean models.

2.2. *LES of stacked shallow water equations*

Equations (2.1)-(2.3) can be spatially filtered $\overline{(\cdot)}$ to arrive at,

$$\partial_t \overline{u} − (\overline{\omega} + f)\,\overline{v} + \partial_x(\overline{K} + \overline{M}) = \overline{\mathcal{F}_x} + \sigma_y, \tag{2.4}$$

$$\partial_t \overline{v} + (\overline{\omega} + f)\,\overline{u} + \partial_y(\overline{K} + \overline{M}) = \overline{\mathcal{F}_y} − \sigma_x, \tag{2.5}$$

$$\partial_t \overline{h} + \partial_x(\overline{u}\overline{h}) + \partial_y(\overline{v}\overline{h}) = −\partial_x\lambda_x − \partial_y\lambda_y, \tag{2.6}$$

where fluid layer index k has been omitted for brevity. Further,

$$\sigma_j = \overline{u_j\omega} − \overline{u}_j\overline{\omega} \quad \text{and} \quad \lambda_j = \overline{u_j h} − \overline{u}_j\overline{h} \quad \text{with} \quad j \in \{1, 2\} \tag{2.7}$$

are the subfilter-scale (SFS) vorticity flux and subfilter thickness fluxes (i.e., mass fluxes), respectively.

The main effort of this work is to parameterize vorticity fluxes. Note that in the momentum equations (Eqs. (2.4) and (2.5)), we neglect the contribution of the subfilter kinetic energy because it does not affect flows with zero horizontal divergence (Marshall & Adcroft 2010). Our approach can be enhanced by parameterizing subfilter momentum fluxes rather than the vorticity fluxes. This adjustment would incorporate the local conservation law of momentum and naturally account for the horizontally divergent flows. However, extracting the momentum fluxes would require applying thickness-weighted averaging (Loose *et al.* 2023), also known as Favre averaging, which was previously adopted for LES of compressible flows by Moin *et al.* (1991).

2.3. *Vorticity closure*

Here we consider the subfilter model of Perezhogin & Glazunov (2023)

$$\overline{u_j\varpi} - \overline{u}_j\overline{\varpi} \approx \overline{\overline{u_j\varpi}} - \overline{\overline{u}_j\overline{\varpi}} + C_S(\Delta x)^4|\overline{S}|\frac{\partial\nabla^2\overline{\varpi}}{\partial x_j} + C_R\left(\overline{\overline{u'_j}\ \overline{\varpi'}} - \overline{\overline{u'_j}}\ \overline{\overline{\varpi'}}\right), \qquad (2.8)$$

which consists of the Leonard flux, biharmonic Smagorinsky model, and the Reynolds-stress model, respectively, where $|\overline{S}| = \sqrt{(\partial_x\overline{u} - \partial_y\overline{v})^2 + (\partial_y\overline{u} + \partial_x\overline{v})^2}$ is the modulus of strain-rate tensor, $\nabla^2 = \partial_x^2 + \partial_y^2$ is the Laplace operator and Δx is the grid spacing of the coarse LES model. Note that for a quantity ϕ, we define $\overline{\phi'} = \overline{\phi} - \overline{\overline{\phi}}$ and $\overline{\overline{\phi'}} = \overline{\overline{\phi}} - \overline{\overline{\overline{\phi}}}$.

2.3.1. *Dynamic estimation of C_S and C_R*

The subfilter closure (Eq. (2.8)) has two free parameters, C_S and C_R, which can be estimated with the dynamic procedure (see Perezhogin & Glazunov 2023, in Appendix D). Herein, we describe only a modification of this dynamic procedure using a scale-similarity dynamic procedure (see Yuan *et al.* 2022, in Section 4.2). In our work, we found that the Yuan *et al.* (2022) dynamic procedure has several advantages as compared to Germano *et al.* (1991), specifically for the MOM6 ocean model: reduced computational cost, higher *a-priori* accuracy and lower sensitivity to the boundary artifacts.

The dynamic procedure of Yuan *et al.* (2022) can be further simplified following Perezhogin & Glazunov (2023) who assume that a test filter $\widehat{(\cdot)}$ equals to the base filter, $\widehat{(\cdot)} \equiv \overline{(\cdot)}$, and thus the subfilter closure on the test-filter level is given in Eq. (2.8). Then, substituting unfiltered fields (u_j, ϖ) with filtered fields $(\overline{u}_j, \overline{\varpi})$ in Eq. (2.8), we obtain an analog of Germano *et al.* (1991) identity for our subfilter closure:

$$\overline{\overline{u_j\varpi}} - \overline{\overline{u}_j\overline{\varpi}} \approx \overline{\overline{\overline{u}_j\overline{\varpi}}} - \overline{\overline{\overline{u}_j}\overline{\overline{\varpi}}} + C_S(\Delta x)^4|\overline{\overline{S}}|\frac{\partial\nabla^2\overline{\overline{\varpi}}}{\partial x_j} + C_R\left(\overline{\overline{\overline{u'_j}\ \overline{\varpi'}}} - \overline{\overline{\overline{u'_j}}}\ \overline{\overline{\overline{\varpi'}}}\right), \qquad (2.9)$$

where for any ϕ we define $\overline{\overline{\phi'}} = \overline{\overline{\phi}} - \overline{\overline{\overline{\phi}}}$ and $\overline{\overline{\overline{\phi'}}} = \overline{\overline{\overline{\phi}}} - \overline{\overline{\overline{\overline{\phi}}}}$. Both LHS and RHS in Eq. (2.9) can be computed given only the resolved fields $(\overline{u}_j, \overline{\varpi})$. Thus, assuming that the optimal free parameters C_S and C_R are equal in Eqs. (2.8) and (2.9), we estimate them from Eq. (2.9) using the least squares minimization:

$$C_S = \frac{\langle(l_j - h_j)m_j\rangle}{\langle m_j m_j\rangle}, \qquad (2.10)$$

$$C_R = \frac{\langle(l_j - h_j - C_S m_j)b_j\rangle}{\langle b_j b_j\rangle}, \qquad (2.11)$$

where $l_j = \overline{\overline{u_j\varpi}} - \overline{\overline{u}_j\overline{\varpi}}$, $h_j = \overline{\overline{\overline{u}_j\overline{\varpi}}} - \overline{\overline{\overline{u}_j}\overline{\overline{\varpi}}}$, $m_j = (\Delta x)^4|\overline{\overline{S}}|\frac{\partial\nabla^2\overline{\overline{\varpi}}}{\partial x_j}$, $b_j = \overline{\overline{\overline{u'_j}\ \overline{\varpi'}}} - \overline{\overline{\overline{u'_j}}}\ \overline{\overline{\overline{\varpi'}}}$, and $\langle\cdot\rangle$ denotes horizontal averaging. Equations (2.10) and (2.11) predict unique coefficients C_S and C_R for every fluid layer and time step. Note that we first estimate the Smagorinsky coefficient C_S (Eq. (2.10)), and only then the backscattering coefficient C_R (Eq. (2.11)) for better numerical stability (see Perezhogin & Glazunov 2023, in Appendix D2).

2.3.2. *Numerical implementation*

We consider the one-dimensional filter of Sagaut & Grohens (1999)

$$\overline{\phi}_i^x = \frac{\epsilon^2}{24}(\phi_{i-1} + \phi_{i+1}) + (1 - \frac{\epsilon^2}{12})\phi_i \qquad (2.12)$$

which has FGR $= \overline{\Delta}/\Delta x = \epsilon \leq \sqrt{6}$. We apply it along two horizontal directions to create a two-dimensional LES filter $\overline{(\cdot)} \equiv \overline{\overline{(\cdot)}^y}^x = \overline{\overline{(\cdot)}^x}^y$. An additional filter with FGR $= \sqrt{12}$ is given by two iterations of two-dimensional filter with $\epsilon = \sqrt{6}$. The boundary values are set to zero for every iteration of the two-dimensional filter. Changing boundary conditions to $\partial_y u = 0$ and $\partial_x v = 0$ when the filter is applied to the velocity field may be favorable to eliminate commutation error with the curl operator near the boundary (not yet implemented in MOM6). The commutation error away from the boundaries is second order in the filter width (Ghosal & Moin 1995) and related to the grid spacing, which is uniform in spherical coordinates but nonuniform in cartesian coordinates.

The inverse direction of the energy cascade in 2D fluids can result in the prediction of a negative Smagorinsky coefficient which may potentially lead to numerical instabilities. This issue is often resolved in 2D fluids by clipping the numerator of Eq. (2.10) before spatial averaging, which is an *ad hoc* approach. In this work, we ensure that C_S is positive and has physically relevant values ($C_S \approx 0.05$) by using an eddy viscosity model that has a positive correlation with subfilter fluxes (biharmonic viscosity model) and by increasing the FGR parameter. Note, however, that we clip Eq. (2.10) after the spatial averaging. This clipping is activated occasionally during a transient startup phase, in the lower fluid layer, and at the coarsest resolutions. Further, the coefficient C_S, as predicted by Eq. (2.10), is passed to the eddy viscosity module of MOM6, which is implemented using momentum fluxes for stability reasons.

We found that C_R, as predicted by Eq. (2.11), is sensitive to the artifacts near the boundary. Therefore, we exclude ten points closest to the boundary from the horizontal averaging operator $\langle \cdot \rangle$, achieving accurate predictions ($C_R \approx 20$). The exclusion of boundary points may be necessary due to the fact that horizontal averaging is performed along non-homogeneous directions (x, y). This issue might be mitigated by employing a localized formulation of the dynamic procedure using Lagrangian averaging (Meneveau *et al.* 1996).

2.4. *Thickness closure*

We propose a new subfilter closure for thickness fluxes following Bardina *et al.* (1980):

$$\lambda_j \approx \overline{\overline{u_j}\,\overline{h}} - \overline{\overline{u}}_j\overline{\overline{h}}. \tag{2.13}$$

The predicted thickness flux is converted to a streamfunction Ψ_j defined on the interfaces (upper and lower) of the fluid layer similar to Gent & McWilliams (1990) as follows: $\Psi_j|_{\text{upper}} - \Psi_j|_{\text{lower}} = \lambda_j$ with the boundary conditions $\Psi_j = 0$ at the ocean surface and floor. Note that such conversion is not unique and may be challenging in vanishing fluid layers. Our implementation is numerically stable as a result of three factors: dissipative numerical scheme for thickness equation, converting thickness fluxes to a streamfunction, and limiting the streamfunction to prevent negative thickness.

3. Results

We evaluate the vorticity closure (Section 2.3) in the Double Gyre configuration of the MOM6 ocean model. Our analysis starts by examining three filter widths $\overline{\Delta}$ (in relation to the Rossby radius), followed by considering three values of the sole input parameter to the subfilter closure, FGR $= \overline{\Delta}/\Delta x$.
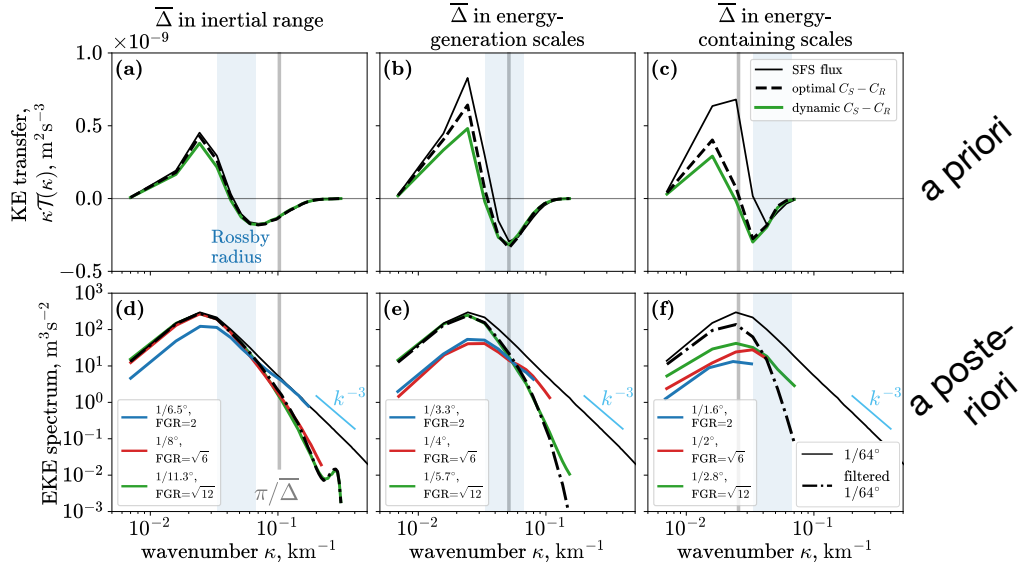
FIGURE 2. Subfilter kinetic energy (KE) transfer in *a-priori* analysis at FGR $= \sqrt{12}$ (a-c) and spatial spectrum in *a-posteriori* simulations at three FGRs (d-f) for vorticity closure described in Section 2.3. The backscatter can be seen as the positive energy transfer in panels (a-c). All spectra correspond to a box $(5°-15°\text{E}) \times (35°-45°\text{N})$ in upper fluid layer. Each column shows a different filter scale $\overline{\Delta}$ denoted with vertical gray line. The dashed line on panels (a-c) shows vorticity closure with parameters C_S and C_R inferred from *a-priori* subfilter flux data σ_j which is not available *a-posteriori*.

3.1. *A-priori accuracy*

The main challenge in parameterizing vorticity fluxes is the need to predict strong kinetic energy backscatter, which appears as a prominent positive energy transfer in large scales (Figure 2(a-c)). The proposed vorticity closure accurately predicts the energy transfer spectrum *a-priori* when the filter scale $\overline{\Delta}$ corresponds to the inertial range of the energy spectrum, see green line in Figure 2(a). However, when the filter scale is outside of the self-similar range, the backscatter prediction is too small compared to the subfilter data, see Figure 2(b,c).

The drop of *a-priori* accuracy can be associated with two alternative reasons. (1) The desired energy transfer cannot be expressed with the subfilter closure (Eq. (2.8)) for any combination of parameters C_S and C_R or (2) dynamic estimation of these parameters is inaccurate when the dynamic procedure is applied outside of the self-similar range. To distinguish between these two reasons, we estimate the optimal values of parameters C_S and C_R by minimizing the mean squared error in the prediction of the subfilter fluxes σ_j diagnosed from the high-resolution simulation. A subfilter closure with optimal parameters is similar to the closure with dynamically estimated parameters, compare dashed and green lines in Figure 2(a-c). Thus, we infer that the drop in *a-priori* accuracy is perhaps due to the first reason. From a physical perspective, subfilter modeling becomes particularly difficult because backscatter occurs already at a filter scale, see Figure 2(c).

3.2. *A-posteriori accuracy*

We report the sensitivity of the *a-posteriori* results to the FGR $= \overline{\Delta}/\Delta x$ parameter. The simulations at FGR $= 2$ have too large energy density in the small scales compared to
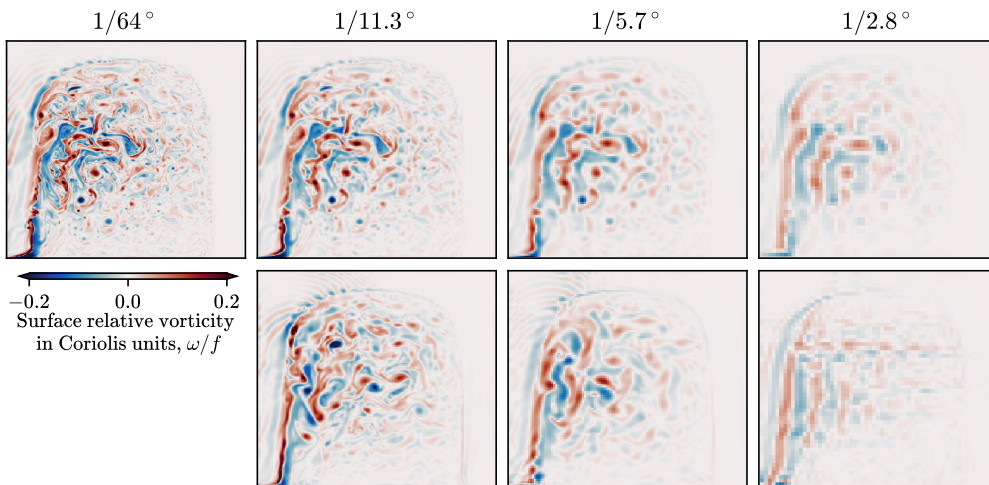
FIGURE 3. Snapshots of the high-resolution model and its filtered versions in upper row and *a-posteriori* simulations with the vorticity closure (Section 2.3) in lower row; FGR = $\sqrt{12}$.

the filtered high-resolution data (Figure 2(d)) mainly because the predicted Smagorinsky coefficient ($C_S \approx 0.00 - 0.01$) is too small compared to a default value of $C_S = 0.06$. We alleviate this issue by increasing the FGR parameter which is possible because the dynamically estimated Smagorinsky coefficient scales as $C_S \sim \overline{\Delta}^4$.

Panels (d) and (e) in Figure 2 demonstrate the success of the explicit filtering approach – the *a-posteriori* LES simulations converge to the filtered high-resolution data when the FGR parameter is increased ($\overline{\Delta}/\Delta x \to \infty$) at a fixed filter scale ($\overline{\Delta}$ = const). However, the rate of convergence of *a-posteriori* simulations depends on the filter scale. When the filter scale corresponds to the inertial range, convergence is achieved at FGR = $\sqrt{6}$ (Figure 2(d)); when the filter scale corresponds to the energy-generation scales (Rossby radius), the convergence requires wider base filter with FGR = $\sqrt{12}$ (Figure 2(e)). Finally, at the largest filter scale convergence to the filtered high-resolution data was not achieved (Figure 2(f)). For snapshots of the solution, see Figure 3.

Here we emphasize that the grid resolutions, at which the convergence to the filtered high-resolution data was observed ($\approx 1/6° - 1/8°$), are enough to simulate the large scales directly, see Figure 1(b). This may lead to a conclusion that the vorticity closure only provides marginal improvements over the biharmonic Smagorinsky model. However, in the remainder of this report we show that the proposed closure has a favorable impact on additional metrics of the mean flow even when using a large FGR or an FGR that is not sufficient to converge to the filtered high-resolution data.

3.3. *Comparison to baseline parameterizations*

Based on the analysis above, we set the FGR parameter to $\sqrt{12}$, which is optimal for the intermediate grid resolutions $\approx 1/4°$, and run simulations for a range of resolutions $1/2° - 1/8°$ (see Figure 4). Our baseline closure, the biharmonic Smagorinsky model, has too large available potential energy (APE), and a significant error in time-mean sea surface height (SSH). The proposed vorticity closure reduces the APE towards the reference value and improves the error in time-mean SSH at all resolutions (Figure 4(b,c)).

We consider another baseline – the momentum closure that was significantly tuned
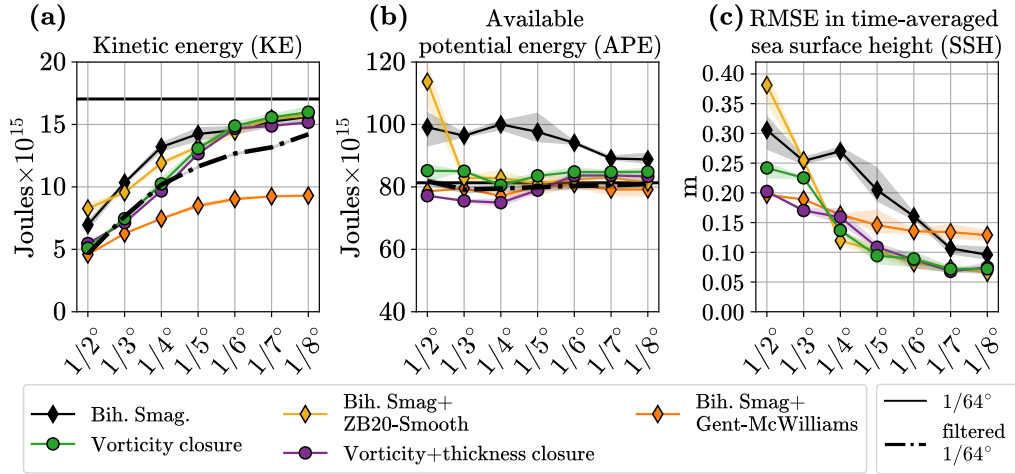
FIGURE 4. Three *a-posteriori* metrics as a function of resolution. Baseline parameterizations: biharmonic Smagorinsky model ($C_S = 0.06$), and its combination with "ZB20-Smooth" (Perezhogin *et al.* 2023) or Gent & McWilliams (1990) (with thickness diffusivity $125\mathrm{m}^2\mathrm{s}^{-1}$). The proposed vorticity (Section 2.3) and combined vorticity+thickness (Sections 2.3, 2.4) closures have FGR = $\sqrt{12}$.

with respect to *a-posteriori* metrics, a modification of the gradient model of Zanna & Bolton (2020), abbreviated as "ZB20-Smooth" (Perezhogin *et al.* 2023). The proposed vorticity closure offers similar performance in all three metrics (KE, APE, error in SSH) as compared to the ZB20-Smooth at resolutions $1/5° - 1/8°$ (Figure 4) but with the advantage of a more transparent tuning procedure. At the coarsest resolution ($1/2°$), the vorticity closure is better in predicting the APE and SSH, although, this improvement can be partially attributed to a small predicted Smagorinsky coefficient at this resolution ($C_S \approx 0.00 - 0.01$). Note that the vorticity closure slightly overestimates the kinetic energy of the filtered high-resolution model at resolutions $1/5° - 1/8°$ (Figure 4(a)).

Further, combining the vorticity closure with the thickness closure reduces the error in SSH at the coarsest resolutions $1/2° - 1/3°$ (Figure 4(c)). Overall, a combined vorticity+thickness closure has a performance comparable to a baseline thickness downgradient parameterization of Gent & McWilliams (1990) at the coarsest resolutions ($1/2°$-$1/3°$) and to the momentum closure of Zanna & Bolton (2020) at the highest resolutions ($1/5° - 1/8°$). Additionally, compared to the Gent & McWilliams (1990) parameterization, the proposed thickness closure does not spuriously reduce the kinetic energy and does not require tuning of the free parameter as a function of resolution (i.e., it is "scale-aware", see Bachman *et al.* 2017).

4. Conclusions

The primary difference between the large-scale ocean dynamics and 3D turbulence is the underlying flow but not the methods that can be used for their analysis and parameterization. In this context, we parameterize mesoscale eddies in GFDL MOM6 ocean model with a lateral subfilter closure of vorticity fluxes by Perezhogin & Glazunov (2023) and improve it with the dynamic procedure of Yuan *et al.* (2022) using explicit filtering.

The successful application of the explicit filtering approach was verified by establishing convergence of the LES ocean simulations to the filtered high-resolution ocean model for sufficiently resolved grids ($1/6° - 1/8°$). We found that contrary to the common practice of increasing the kinetic energy while invoking subfilter closures (to capture backscatter), this is not necessary in our configuration. This is primarily because the filter applied to the high-resolution data assigns a significant portion of the kinetic energy to the subfilter scales at practical FGR ($\sqrt{12}$).

We also show that the proposed vorticity closure is accurate in predicting the potential energy and time-mean sea surface height across a range of resolutions ($1/2° - 1/8°$), achieving similar or better results than a recently suggested parameterization (Perezhogin *et al.* 2023). We also report the limitations in the proposed model when the filter scale approaches the energy-containing scales (the *a-priori* performance worsens and *a-posteriori* results do not converge to the filtered high-resolution data). These issues may stem from the need to use a large FGR at coarse resolution, which increases the spatial extent of the subfilter closure. Future work should focus on developing more localized in-space closures that can accurately capture subfilter fluxes at coarse resolution.

Finally, we show that the LES methods can be successfully applied for the prediction of thickness fluxes and propose a model of Bardina *et al.* (1980) for this purpose. It further improves the mean flow at the coarsest resolutions ($1/2° - 1/3°$) without spuriously reducing the KE and thus may be a good alternative to Gent & McWilliams (1990) parameterization.

Acknowledgments

REFERENCES

ADCROFT, A., ANDERSON, W., BALAJI, V., BLANTON, C., BUSHUK, M., DUFOUR, C. O., DUNNE, J. P., GRIFFIES, S. M., HALLBERG, R., HARRISON, M. J. *et al.* 2019 The gfdl global ocean and sea ice model om4. 0: Model description and simulation features. *Journal of Advances in Modeling Earth Systems* **11** (10), 3167–3211.

BACHMAN, S. D., FOX-KEMPER, B. & PEARSON, B. 2017 A scale-aware subgrid model for quasi-geostrophic turbulence. *Journal of Geophysical Research: Oceans* **122** (2), 1529–1554.

BARDINA, J., FERZIGER, J. & REYNOLDS, W. 1980 Improved subgrid-scale models for large-eddy simulation. In *13th fluid and plasmadynamics conference*, p. 1357.

BOSE, S. T., MOIN, P. & YOU, D. 2010 Grid-independent large-eddy simulation using explicit filtering. *Physics of Fluids* **22** (10).

CARATI, D., WINCKELMANS, G. S. & JEANMART, H. 2001 On the modelling of the subgrid-scale and filtered-scale stress tensors in large-eddy simulation. *Journal of Fluid Mechanics* **441**, 119–138.

Fox-Kemper, B. & Menemenlis, D. 2008 Can large eddy simulation techniques improve mesoscale rich ocean models? *Geophysical Monograph Series* **177**, 319–337.

Gent, P. R. & McWilliams, J. C. 1990 Isopycnal mixing in ocean circulation models. *Journal of Physical Oceanography* **20** (1), 150–155.

Germano, M. 1986 A proposal for a redefinition of the turbulent stresses in the filtered navier-stokes equations. *Physics of Fluids* **29** (7), 2323–2324.

Germano, M., Piomelli, U., Moin, P. & Cabot, W. H. 1991 A dynamic subgrid-scale eddy viscosity model. *Physics of Fluids A: Fluid Dynamics* **3** (7), 1760–1765.

Ghosal, S. & Moin, P. 1995 The basic equations for the large eddy simulation of turbulent flows in complex geometry. *Journal of Computational Physics* **118** (1), 24–37.

Horiuti, K. 1997 A new dynamic two-parameter mixed model for large-eddy simulation. *Physics of Fluids* **9** (11), 3443–3464.

Jansen, M. F. & Held, I. M. 2014 Parameterizing subgrid-scale eddy effects using energetically consistent backscatter. *Ocean Modelling* **80**, 36–48.

Khani, S. & Dawson, C. N. 2023 A gradient based subgrid-scale parameterization for ocean mesoscale eddies. *Journal of Advances in Modeling Earth Systems* **15** (2), e2022MS003356.

Loose, N., Marques, G. M., Adcroft, A., Bachman, S., Griffies, S. M., Grooms, I., Hallberg, R. W. & Jansen, M. F. 2023 Comparing two parameterizations for the restratification effect of mesoscale eddies in an isopycnal ocean model. *Journal of Advances in Modeling Earth Systems* **15** (12), e2022MS003518.

Marshall, D. P. & Adcroft, A. J. 2010 Parameterization of ocean eddies: Potential vorticity mixing, energetics and arnold's first stability theorem. *Ocean Modelling* **32** (3-4), 188–204.

Meneveau, C., Lund, T. S. & Cabot, W. H. 1996 A lagrangian dynamic subgrid-scale model of turbulence. *Journal of fluid mechanics* **319**, 353–385.

Moin, P., Squires, K., Cabot, W. & Lee, S. 1991 A dynamic subgrid-scale model for compressible turbulence and scalar transport. *Physics of Fluids A: Fluid Dynamics* **3** (11), 2746–2757.

Perezhogin, P. & Glazunov, A. 2023 Subgrid Parameterizations of Ocean Mesoscale Eddies Based on Germano Decomposition. *Journal of Advances in Modeling Earth Systems* **15** (10).

Perezhogin, P., Zhang, C., Adcroft, A., Fernandez-Granda, C. & Zanna, L. 2023 Implementation of a data-driven equation-discovery mesoscale parameterization into an ocean model. *arXiv preprint arXiv:2311.02517* .

Sagaut, P. & Grohens, R. 1999 Discrete filters for large eddy simulation. *International Journal for Numerical Methods in Fluids* **31** (8), 1195–1220.

Winckelmans, G. S., Wray, A. A., Vasilyev, O. V. & Jeanmart, H. 2001 Explicit-filtering large-eddy simulation using the tensor-diffusivity model supplemented by a dynamic smagorinsky term. *Physics of Fluids* **13** (5), 1385–1403.

Yuan, Z., Wang, Y., Xie, C. & Wang, J. 2022 Dynamic nonlinear algebraic models with scale-similarity dynamic procedure for large-eddy simulation of turbulence. *Advances in Aerodynamics* **4** (1), 16.

Zanna, L. & Bolton, T. 2020 Data-driven equation discovery of ocean mesoscale closures. *Geophysical Research Letters* **47** (17), e2020GL088376.